High temperature spin crossover behaviour of mononuclear bis-(thiocyanato)iron(ii) complexes with judiciously designed bidentate N-donor Schiff bases with varying substituents

Kishalay Bhar, Wenbin Guo, Mathieu Gonidec, Venkata Nikhil Raj M, Surabhi Bhatt, Franc Perdih, Philippe Guionneau, Guillaume Chastanet, Anuj Sharma

Revision#1 Manuscript ID: DT-ART-02-2022-000416

High temperature spin crossover behaviour of mononuclear *bis*-(thiocyanato)iron(II) complexes with judiciously designed bidentate N-donor Schiff bases with varying substituent

Kishalay Bhar,[a] Wenbin Guo,[b] Mathieu Gonidec,[b] Venkata Nikhil Raj M.,[a] Surabhi Bhatt,[a] Franc Perdih,[c] Philippe Guionneau,*[b] Guillaume Chastanet,*[b] and Anuj K. Sharma*[a]

Presented herein a family of molecular *cis*-[Fe^{II}(X-PPMA)$_2$(NCS)$_2$]•H_2O [4-X-N-(phenyl(pyridin-2-yl)methylene)aniline; X-PPMA; X = -Cl (**1**), -Br (**2**), -CH_3 (**3**)] complexes that exhibit spin crossover behaviour above room temperature. Judiciously designed bidentate N-donor Schiff bases of 2-benzoylpyridine and para-substituted anilines in combination with Fe(NCS)$_2$ were used for the synthesis of complexes **1-3**. The relatively strong ligand field of the Schiff bases stabilises the low spin state of ion(II) upto 300 K which is evident from magnetic measurements, room temperature Mössbauer spectra and crystallographic bond/angle distortion parameters. Interestingly, complexes **1-3** crystallize in a tetragonal system with a chiral space group either $P4_32_12$ or $P4_12_12$ from achiral building units due to supramolecular helical arrangements of molecules through intermolecular (pyridine)C-H···C(NCS) interactions in crystalline state. Complexes **1** and **2** exhibit complete, gradual and slightly irreversibile spin crossover behaviour over the temperature range 300-500 K with equilibrium temperatures ($T_{1/2}$) 375 K (**1**) and 380 K (**2**). Spin state evolution of iron(II) in complexes **1** and **2** is monitored between 150 K and 450 K through variable temperature crystallographic studies on warming mode. The structural data are in good agreement with the 94% (**1**) and 87% (**2**) high spin conversion of iron(II) at 450 K. At high temperature (450 K), some minor irreversible ligand motion is noticed in complexes **1** and **2**, in addition to a complete solvent loss, that may induce the slight irreversibility of the spin crossover. On the other hand, complex **3** shows a complete and gradual spin crossover in the temperature range 10-475 K with strong irreversible features. The equilibrium temperatures obtained upon first warming ($T_{1/2}\uparrow$) and second cooling ($T_{1/2}\downarrow$) are 375 K and 200 K, respectively. In complex **3**, the loss of water molecule triggers the strong deviations in spin crossover behaviour.

[a] *Department of Chemistry, School of Chemical Sciences and Pharmacy, Central University of Rajasthan, NH-8, Bandarsindri, Ajmer Distt. Rajasthan-305817 India.*

[b] *Univ. Bordeaux, CNRS, Bordeaux INP, ICMCB, UMR 5026, 87 avenue du Dr A. Schweitzer, F-33600 Pessac, France.*

[c] *Faculty of Chemistry and Chemical Technology, University of Ljubljana, Vecna pot 113, PO Box 537, SI-1000 Ljubljana, Slovenia.*

† Corresponding Authors

*E-mail for P.G.: philippe.guionneau@u-bordeaux.fr

*E-mail for G.C.: guillaume.chastanet@icmcb.cnrs.fr

*E-mail for A.K.S.: anuj.sharma@curaj.ac.in

Electronic Supplementary Information (ESI) available: [details of any supplementary information available should be included here]. See DOI: 10.1039/x0xx00000x

Introduction

Spin state switching [Low Spin (LS) ↔ High Spin (HS)] triggered by external perturbations (T, P, hυ) in spin crossover (SCO)[1-3] molecules leads to changes in magnetic moment, conductivity, dielectric constant and even colour of the material. This makes SCO materials suitable for applications as molecular switches or memories in information and sensor devices.[1, 4-8] In general, transition metal complexes with electronic configurations $3d^n$ (n = 4-7) in suitable octahedral coordination environments are known to exhibit SCO phenomenon.[1] Among them, iron(II) ($3d^6$) SCO complexes are widely studied due to their remarkable change in magnetic and optical properties during the electronic transition from the diamagnetic (S = 0, t_{2g}^6, $^1A_{1g}$) LS state to the paramagnetic (S = 2, $t_{2g}^4e_g^2$, $^5T_{1g}$) HS state.[1] In the solid state, the SCO behaviour of a molecule is primarily defined by two well-known parameters such as its transition temperature ($T_{1/2}$) and cooperativity.

The transition temperature ($T_{1/2}$),[1] defined as the temperature at which the ratio of HS and LS fractions are equal, depends upon coordinated ligand environment around the metal centre. It is evident that weak field ligand stabilising the HS state of metal ion results in low $T_{1/2}$ value. On contrary, a strong ligand field stabilises the LS state and the $T_{1/2}$ value shifts towards the higher temperature region.[9] Thus to achieve spin transition near room temperature for SCO molecules, judiciously designed ligands frameworks that can stabilise the LS state are required. Properly designed Schiff bases[10] are well-suited for this purpose because of their ease of preparation and versatility in ligand framework, where the ligand field can be easily fine-tuned by smart variation of the amine and carbonyl components.

The cooperativity[11-14] in SCO systems may be defined as how effectively the local change in spin state at the metal site is transmitted among the spin active metal ions *via* non-covalent and/or covalent bonds throughout the crystal lattice, in a multiscale description.[15, 16] The SCO behaviour of molecules is markedly varied from gradual to abrupt to hysteretic with the improvement of cooperative elastic interactions between the molecules. In literature SCO behaviours of *cis*-$[Fe^{II}(L)_2(NCS)_2]$ complexes containing the bidentate N-donor ligands (L) are well documented.[17-25] In this regard, complexes related to Schiff bases of pyridine-2-carboxaldehyde and *para*-substituted anilines [substituted-N-(2′-pyridylmethylene)aniline; PM-L, L = phenyl, biphenyl, phenylethyne, phenylazo, naphthylethyne, **Scheme 1**] are particularly interesting as they exhibit a varied range of SCO behaviours (gradual → abrupt → hysteresis) albeit below room temperature. In such PM-L based complexes, the para-substituent of aniline plays an important role on the nature of the spin crossover. The cooperativity in this molecular system arises primarily due to hydrogen bonds (particularly S···H-C contact) as well as π-π stacking and difference in the packing arrangements.[16, 18-20] In this endeavour, a new series of bidentate N-donor Schiff bases [4-X-N-(phenyl(pyridin-2-yl)methylene)-aniline; X-PPMA; X = -Cl, -Br, $-CH_3$; **Scheme 1**] have been synthesised using 2-benzoylpyridine and aniline derivatives (4-chloroaniline, 4-bromoaniline and 4-methylaniline) for molecular *cis*-$[Fe(L)_2(NCS)_2]$ system to obtain spin crossover near or above room temperature region. In X-PPMA, a phenyl group is introduced in place of imine H of PM-L ligand to enhance the electronic conjugation in the ligand framework (**Scheme 1**) for effective stabilisation of LS state of iron(II).[9] In addition, we have also varied the *para*-substituent of the aniline derivative from Cl→Br→CH_3 to explore their effect on SCO behaviour.[26] Successfully, three new iron(II) complexes of type *cis*-$[Fe(X\text{-}PPMA)_2(NCS)_2]\bullet H_2O$ [4-X-N-(phenyl(pyridin-2-yl)methylene)aniline; X-PPMA; X = -Cl (**1**), -Br (**2**), $-CH_3$ (**3**); **Scheme 1**] have been isolated. All the complexes are in LS state at room temperature and exhibit gradual spin crossover behaviour above 300 K. Interestingly, the spin crossover features of complexes **1-3** varied drastically depending on the nature of the substituent (Cl/Br→CH_3). The details of synthesis, spectroscopic characterizations, room temperature structures, temperature induced spin crossover behaviour, variable temperature crystal structures, and magneto-structural correlations of complexes **1-3** are discussed herein.

Scheme 1 Structures of the reported PM-L ligands, newly synthesized X-PPMA Schiff bases and molecular *cis*-[Fe(X-PPMA)$_2$(NCS)$_2$].H$_2$O complexes.

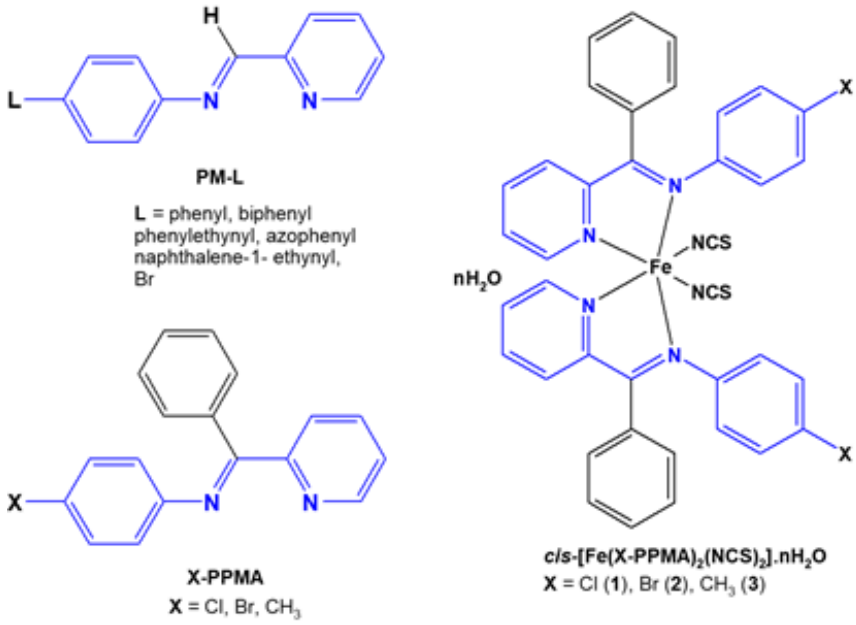

Results and discussion

Synthesis and characterization

Three new bidentate N-donor Schiff bases (**Cl-PPMA**, **Br-PPMA** and **CH$_3$-PPMA**) were synthesized by refluxing 1:1 molar ratio of 2-benzoylpyridine and the corresponding aniline derivative (4-chloroaniline, 4-bromoaniline and 4-methylaniline) in methanol for 24 h. All the ligands were characterized by ESI-MS and ^{1}H-NMR spectroscopy (*see experimental section*). Complexes (**1-3**) were isolated in dark blue crystalline form by mixing 2:1 molar ratio of the respective Schiff bases and Fe(NCS)$_2$ (*prepared in-situ see experimental section*) in methanol under nitrogen atmosphere at room temperature. The composition of complexes (**1-3**) was ascertained by elemental analyses and spectroscopic studies (*see experimental section*). In the FTIR spectra, complexes **1-3** shows the characteristic bands of *cis*-oriented nitrogen bonded thiocyanate ν(C≡N) around 2100 and 2057 cm^{-1} and peaks of Schiff bases ν(C=N + C=C) in the range 1625-1470 cm^{-1} (*see experimental section*).

Room temperature characterizations

The spin state of iron(II) in **1-3** was determined through room temperature Mössbauer and crystallographic studies.

Room temperature Mössbauer studies on **1-3** reveal one doublet with relatively low values of quadrupole splitting (ΔE_Q < 1 mm/s) and isomer shift (δ < 0.5 mm/s) parameters (**Table S1; Figure S1**) which are attributed to the LS state ($^1A_{1g}$) of iron(II).[27]

The structural data for **1-3** at 293(2) K (**1**^{RT}, **2**^{RT} and **3**^{RT}) reveals complexes **1-3** crystallize in tetragonal system with a chiral space group either $P4_32_12$ (**1**) or $P4_12_12$ (**2** and **3**) as a mixture of two possible enantiomers (Λ or Δ) in bulk sample.[28-30] **1-3** contain [Fe(**X-PPMA**)$_2$(NCS)$_2$] molecular unit (X = Cl for **1**, Br for **2** and CH_3 for **3**) (**Table S2**). Electron density associated with disordered solvent molecules was removed by solvent mask. Therefore, the chemical formula and crystal data given in Table S2 do not take into account these solvent molecules. In each complex, the iron(II) centre is located on the two-fold rotation axis adopting a pseudo-octahedral geometry (**Figure 1**). The iron(II) centre is coordinated by two pyridine N atoms (N1 and N1^i), two imine N atoms (N2 and N2^i) of two bidentate Schiff bases (**Cl-PPMA** for **1**, **Br-PPMA** for **2** and **CH$_3$-PPMA** for **3**) along with two *cis*-oriented thiocyanato N atoms (N3 and N3^i) (symmetry code: (i) *x*, *y*, –*z* + 1). The equatorial plane is formed by two imine N atoms and two thiocyanato N atoms. The axial sites are occupied with two pyridine N atoms. The average Fe-N distances are 1.9669 Å for **1**, 1.9703 Å for **2** and 1.9651 Å for **3** (**Table S3**), strongly suggesting a LS state of iron(II) in **1-3**. The distortion around the iron(II) centre is calculated in terms of angle distortion parameters[15, 16, 31] [Σ represents the sum of the deviations from 90° of the 12 cis N–Fe–N angles in the FeN_6 coordination sphere, $\sum = \sum_i^{12} |90 - \alpha_i|$: 43.8° for **1**, 44.5° for **2** and 42.8° for **3** and Θ represents the deviation of the FeN_6 geometry from perfectly octahedral (O_h) to a trigonal prismatic structure (D_{3h}): 137° for **1**, 136° for **2** and 138° for **3**] and length distortion parameter [ζ represents the sum of the deviations from the average value of all the Fe-N bond lengths: 0.041 Å for **1**, 0.027 Å for **2** and 0.033 Å for **3**]. All these parameters are also in line with the LS state of iron(II).

Figure 1 View of molecular structures of complexes (a) **1** (b) **2** and (c) **3** at room temperature.

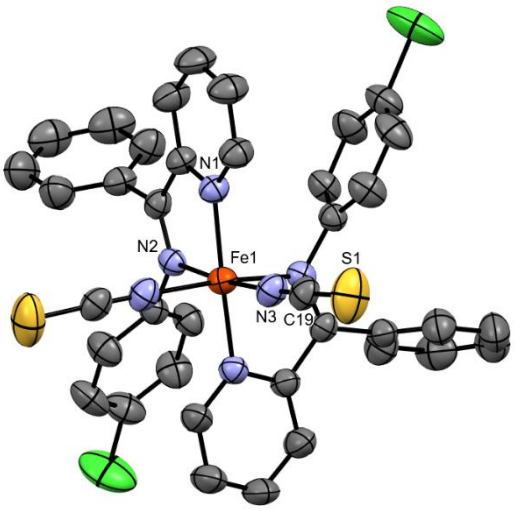

(a)

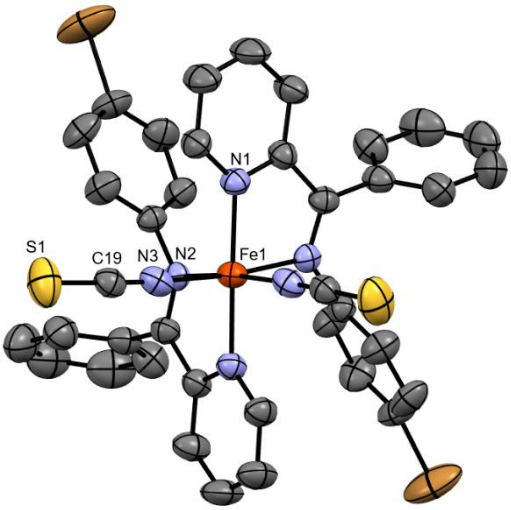

(b)

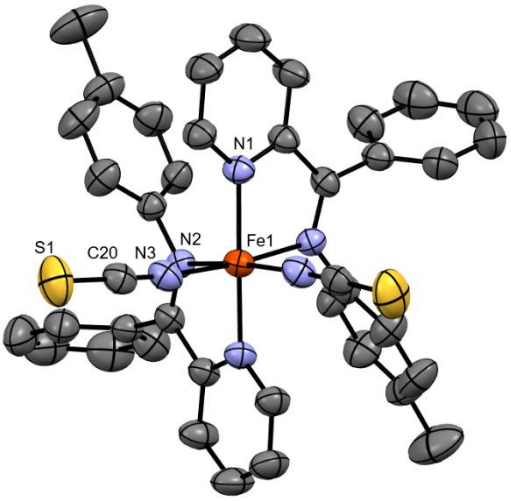

(c)

In addition, the powder-XRD data of complexes **1-3** at 298 K were collected. The PXRD patterns are in good correlation with the SC-XRD data (**Figures S2-S4**).

Variable temperature magnetic susceptibility studies of 1-3

Variable-temperature magnetic susceptibility measurements were carried out on crystalline samples between 10-500 K for **1** and 10-475 K for **2** and **3**. The temperature dependent $\chi_M T$ plots (χ_M being the molar magnetic susceptibility, **Figures 2** and **3**) show that complexes **1** and **2** undergo complete but non-cooperative spin crossover above room temperature. The observed $\chi_M T$ value remains close to 0-0.2 $cm^3.K.mol^{-1}$ in the temperature range of 10-300 K clearly indicative of LS state of iron(II). This is consistent with room temperature Mössbauer spectra and crystallographic bond/angle distortion parameters. Upon further warming the samples, their $\chi_M T$ values gradually increase and reach a maximum of 3.0 $cm^3.K.mol^{-1}$ at 500 K (**1**) and 475 K (**2**) expected for an iron(II) ion in its HS state. Upon cooling the samples down to 250 K, the $\chi_M T$ value decrease again gradually to 0.2-0.3 $cm^3.K.mol^{-1}$ with slight deviation for both **1** and **2** (**Figures 2** and **3**). The average spin crossover temperature ($T_{1/2}$) is found to be around 375 K for **1** and 380 K for **2**. No photoswitching effect at 10 K is observed for these two compounds whatever the wavelength used between 405 and 980 nm.

Figure 2 Temperature dependence of $\chi_M T$ product for **1** recorded on the SQUID magnetometer (o) and VSM (green line first cycle and red line second cycle).

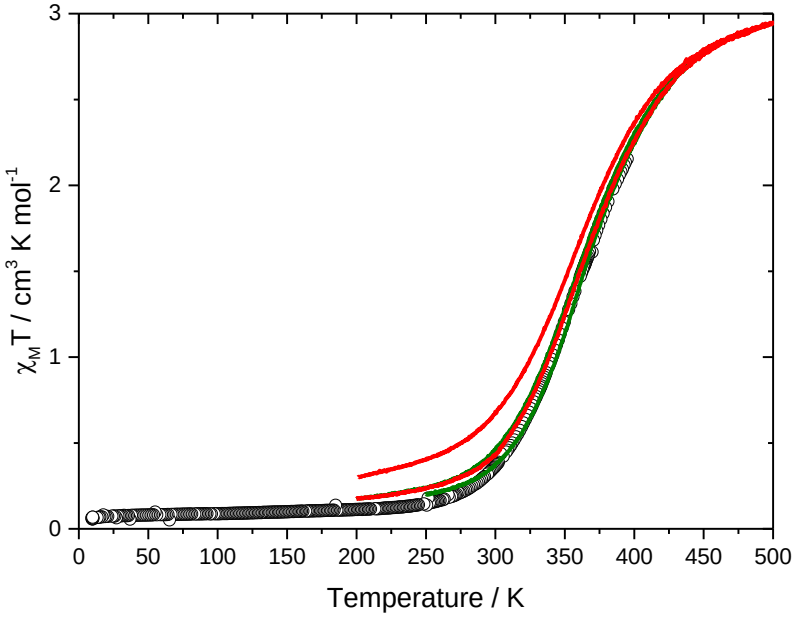

Figure 3 Temperature dependence of $\chi_M T$ product for **2** recorded on the VSM (green line first cycle, red line second cycle, black line fourth cycle and orange line sixth cycle).

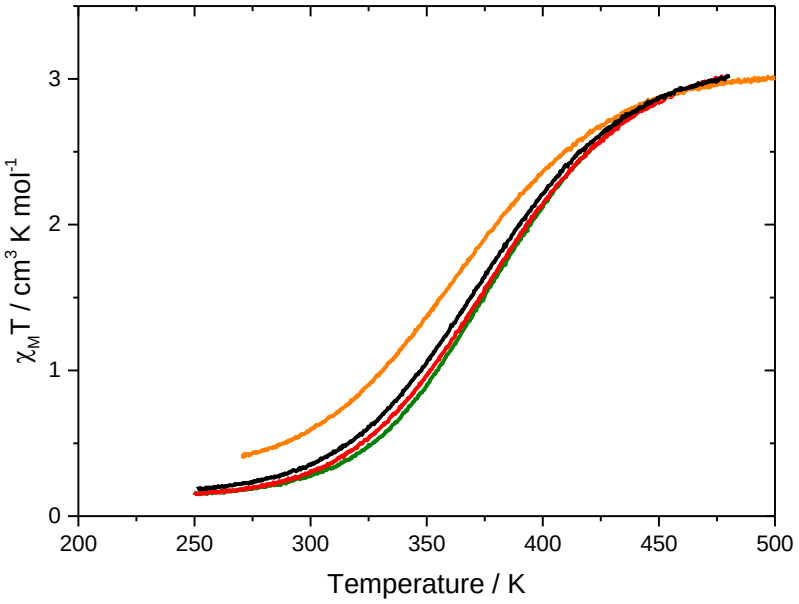

Regarding complex **3**, the temperature dependent $\chi_M T$ plot (**Figure 4** combines SQUID and VSM measurements) shows that it exhibits a complete and non-cooperative spin crossover above room temperature with strong irreversible features. The $\chi_M T$ value remains close to 0-0.2 cm^3.K.mol^{-1} between 10-300 K suggesting LS state of iron(II) as evident from room temperature Mössbauer spectra and

crystallographic bond/angle distortion parameters. Upon first warming of the sample from 300-450 K, the $\chi_M T$ value gradually increases until it reaches a maximum value of 3.0 $cm^3.K.mol^{-1}$ at 450 K as expected for a HS iron(II) ion. Upon first cooling of the sample down to 250 K, the $\chi_M T$ product decreases more gradually following a different path and reaches a value of 1.8 $cm^3.K.mol^{-1}$ indicating 60% iron(II) ions in HS state. Upon second warming up to 475 K, $\chi_M T$ value increases to 3.1 $cm^3.K.mol^{-1}$ following the first cooling path and upon second cooling $\chi_M T$ value remains same up to 300 K indicative of expected HS state of iron(II). With further decrease in temperature from 300-10 K, $\chi_M T$ value decreases to 0.38 $cm^3.K.mol^{-1}$ following a different path compared to first cooling. This value corresponds to around 10% HS state of iron(II) ions. This last curve is reversible upon further warming. The average spin crossover temperatures are around $T_{1/2}$ ↑(1^{st} warming) 375 K and $T_{1/2}$ ↓(2^{nd} cooling) 200 K. Additionally, the original hydrated sample of complex **3** was heated in an oven at 480 K outside SQUID and then magnetic measurement was performed by cooling the sample from 300 K to 10 K. The cooling path is identical with the second cooling curve of the previous measurement. When a 830 nm light irradiation is applied at 10 K on a fresh sample, no photoswitching is observed, while after thermal treatment at 450 K, around 40% of conversion is recorded, witnessing the occurrence of the LIESST effect.[32] The photo-induced state can be erased upon warming at 0.5 K/min above 80 K, with a relaxation temperature T(LIESST) = 60 K.[33, 34]

Figure 4 Temperature dependence of $\chi_M T$ product for **3** recorded on the SQUID magnetometer (o first warming, □ after 1h in an oven at 480 K) and VSM (green line first cycle, red line second cycle and black line third cycle). Behaviour of **3** after thermal treatment at 450 K (1h in an oven) under 830 nm light irradiation (Δ) and after (■).

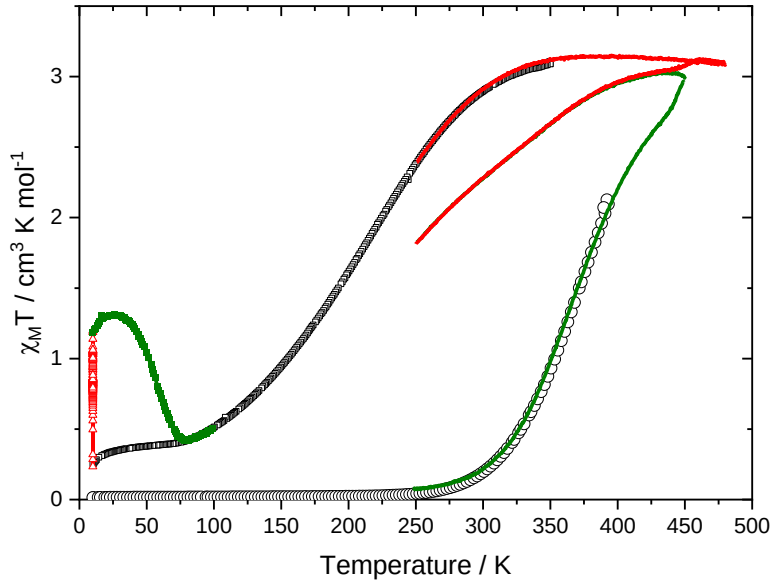

Mononuclear *bis*-(thiocyanato)iron(II) spin crossover complexes of formula $[Fe(L)_n(NCS)_2]$ generally exhibit the equilibrium temperature ($T_{1/2}$) below room temperature region.[17-25] The bidentate Schiff bases, PM-L (**Scheme 1**) containing pyridine-2-carboxyaldehyde and aniline derivatives are widely used in literature (**Table 1**, Sl. No 1-9). In X-PPMA, one phenyl group is introduced instead of the imine hydrogen of PM-L Schiff bases (**Scheme 1**). The presence of phenyl group enhances the conjugation in X-PPMA ligand system, strengthening the ligand field as compared to the other PM-L ligands, and stabilises the LS state of iron(II) up to 300 K. As a result, complexes **1-3** show temperature induced gradual spin crossover behaviour above 300 K (**Table 1**, Sl. No 10-12) with some irreversible features. While complexes **1** and **2** do not exhibit any photoswitching at low temperature, complex **3** does after warming at 450 K. According to the linear T(LIESST) *vs* $T_{1/2}$ relationship reported for the spin crossover complexes ($T(LIESST) = T_0 - 0.3T_{1/2}$),[33, 34] these $[Fe(L)_n(NCS)_2]$ complexes are often lying on a $T_0 = 120$ K line. Complexes **1** and **2** are characterized by quite high $T_{1/2}$ (above 350 K) which supports the absence of LIESST effect on these complexes. Complex **3** after thermal treatment has a $T_{1/2}$ of 200 K which perfectly supports the observation of a T(LIESST) temperature of 60 K.

An important feature of these new compounds is that they crystallize with solvent molecules, which is not the case for the other complexes and polymorphs. The loss of solvent might be at the origin of the irreversible behaviours recorded. Therefore, thermo-gravimetric analyses (TGA) and variable temperature X-ray studies were performed.

Table 1 Spin crossover data for *bis*-(thiocyanato)iron(II) complexes with reported PM-L ligands[17-25] and complexes **1-3**

Sl. No.	Complexes	SCO behaviour/$T_{1/2}$/ΔT
1.	$[Fe(PM\text{-}PEA)_2(NCS)_2]$[21]	Hysteresis and reversible/$T_{1/2}\downarrow$=194 K, $T_{1/2}\uparrow$= 231 K/ΔT = 42 K
2.	$[Fe(PM\text{-}PEA)_2(NCSe)_2]$-I[18]	Hysteresis and reversible/$T_{1/2}\downarrow$= 266 K, $T_{1/2}\uparrow$= 307 K/ΔT = 41 K
3.	$[Fe(PM\text{-}PEA)_2(NCSe)_2]$-II[19]	Gradual and reversible/$T_{1/2}$ = 245 K
4.	$[Fe(PM\text{-}BiA)_2(NCS)_2]$-II[22]	Abrupt and reversible/$T_{1/2}\downarrow$=168 K, $T_{1/2}\uparrow$= 173 K/ΔT = 5 K
5.	$[Fe(PM\text{-}BiA)_2(NCS)_2]$-I[25]	Gradual and reversible/$T_{1/2}$ = 198 K
6.	$[Fe(PM\text{-}TeA)_2(NCS)_2]$[23]	Gradual and reversible/ $T_{1/2}\downarrow$=186 K, $T_{1/2}\uparrow$= 192K/ΔT = 6K
7.	$[Fe(PM\text{-}AzA)_2(NCS)_2]$[23]	Gradual and reversible/ $T_{1/2}\downarrow$=186 K, $T_{1/2}\uparrow$= 192K/ΔT = 6K
8.	$[Fe(PM\text{–}NEA)_2(NCS)_2]$[24]	Very gradual and reversible/$T_{1/2}$ = 204 K
9.	$[Fe(PM\text{-}p\text{BrA})_2(NCS)_2]$-I[20]	Abrupt and reversible/ $T_{1/2}\downarrow$=170.2 K, $T_{1/2}\uparrow$= 181.4 K/ΔT = 11.2 K
10.	$[Fe(Cl\text{-}PPMA)_2(NCS)_2].H_2O$(**1**)	Gradual and slightly irreversible/$T_{1/2}$ = 375 K
11.	$[Fe(Br\text{-}PPMA)_2(NCS)_2].H_2O$(**2**)	Gradual and slightly irreversible/$T_{1/2}$ = 380 K
12.	$[Fe(CH_3\text{-}PPMA)_2(NCS)_2].0.75H_2O$(**3**)	Gradual and strongly irreversible/ $T_{1/2}\uparrow$(1st warming) = 375 K and $T_{1/2}\downarrow$(2nd cooling) = 200 K

PM-PEA = N-(2′-pyridylmethylene)-4-(phenylethynyl)aniline; PM-BiA = N-(2-pyridylmethylene)aminobiphenyl; PM-TeA = N-(2'-pyridylmethylene)-4-(aminoterphenyl); PM-AzA = N-(2'-pyridylmethylene)-4-(phenylazo)aniline; PM–NEA = N-(2-pyridylmethylene)-4-(naphthalene-1-ethynyl)aniline; PM-*p*BrA = N-(2'-pyridylmethylene)-4-bromoaniline.

Thermogravimetric analyses of 1-3

Thermogravimetric analyses (TGA) of complexes **1-3** were made between 30 and 800 °C in the static atmosphere of nitrogen to examine their thermal stabilities. TG curve (**Figure S6**) indicates that complexes **1-3** are stable respectively up to 231 °C, 232 °C and 272 °C, and then decompose gradually up to 800 °C. Complexes **1** and **2** show a gradual weight loss (observed: 2.1%, calculated: 2.3% for **1**; **Figure S7**; observed: 1.9%, calculated: 2.0% for **2**; **Figure S8**) in the temperature range 60-140 °C and 60-122 °C, respectively corresponding to a water molecule. However, for complex **3** the water molecule is released in two steps in the temperature range 72-177 °C and 177-203 °C (observed: 2.38% and calculated: 2.4%; **Figure 5**).

Figure 5 TGA plot and loss of water in complex **3**.

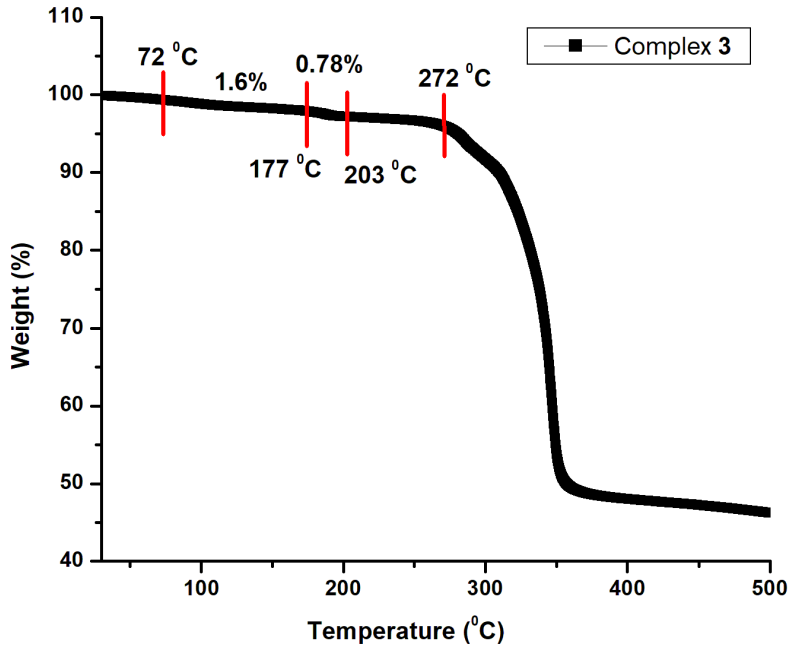

Variable-temperature crystallographic studies of 1-3

To establish magneto-structural correlations, variable-temperature crystallographic data were collected for complexes **1-3**. The crystal structures of **1** and **2** were determined at 150 K (**1/2**$^{\mathbf{150K}}$), 250 K (**1/2**$^{\mathbf{250K}}$), 300 K (**1/2**$^{\mathbf{300K}}$), 350 K (**1/2**$^{\mathbf{350K}}$), 400 K (**1/2**$^{\mathbf{400K}}$), 450 K (**1/2**$^{\mathbf{450K}}$) in warming mode. The complexes crystallise in tetragonal system with a chiral space group either $P4_32_12$ (for **1**) or $P4_12_12$ (for **2**) (**Tables S4** and **S5**). The spin state of iron(II) is determined based on variable-temperature (150-450 K) structural evidences such as <Fe-N> bond length, bond length distortion (ζ) and bond angle distortion (Σ, Θ) parameters (**Tables S6** and **S7**). It is observed that iron(II) is in LS state between 150-300 K. A smooth spin conversion from LS to HS state occurs in 300-450 K temperature range in complexes **1** and **2**. The evolutions of the coordination sphere parameters (Fe-N bond, ζ, Σ, Θ) as a function of temperature (150 K to 450 K) are plotted for **1** (**Figure 6a**) and **2** (**Figure 6b**). At 450 K, the HS conversion is 94% (for **1**) and 87% (for **2**) which is in good agreement with the observed magnetic data (2.8 $cm^3.K.mol^{-1}$ for **1**: 93% HS and 2.7 $cm^3.K.mol^{-1}$ for **2**: 90% HS). Each crystalline water molecule is connected to one coordination complex through weak O···H-C hydrogen bonds (**Figure 7a**). Structural data as well as TG analyses clearly indicate that the crystalline water molecule present in the complexes is lost above 400 K (**1**) and 350 K (**2**). After de-hydration, a slight ligand motion in **1** and **2** is noticed between structures at 150 K and 450 K (**Figures 6a** and **6b**). Both the

de-hydration and this ligand motion may explain the slight deviation in spin crossover behaviour in **1** and **2** between the first warming and the other thermal cycles, since it may alter the intermolecular interactions.

Figure 6 Thermal evolution of coordination sphere parameters for (a) **1** and (b) **2** (lines are guides for the eyes).

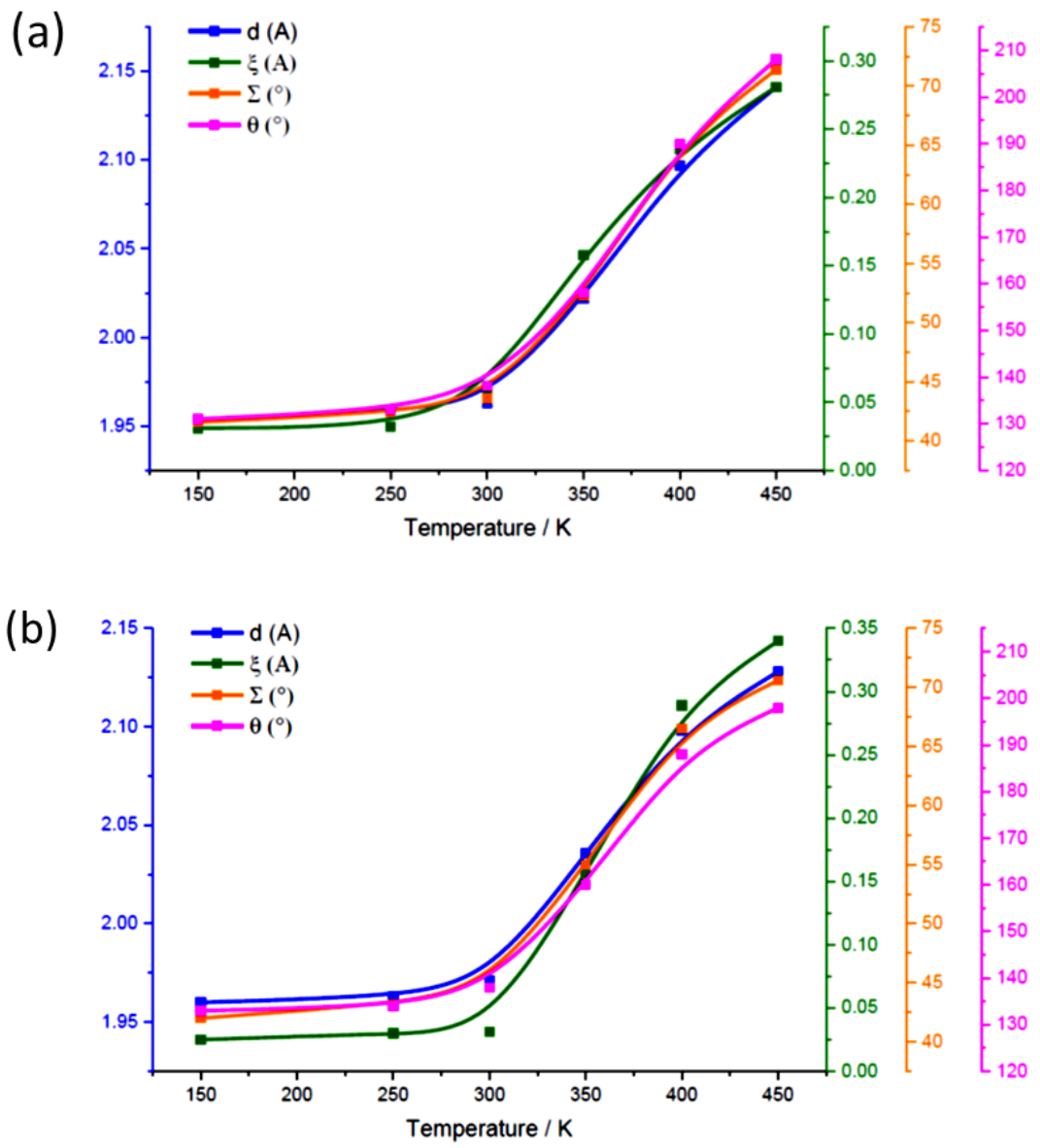

Figure 7 Superposition of the molecular structures at 450 K(red) and 150 K(blue) for (a) **1** and (b) **2**.

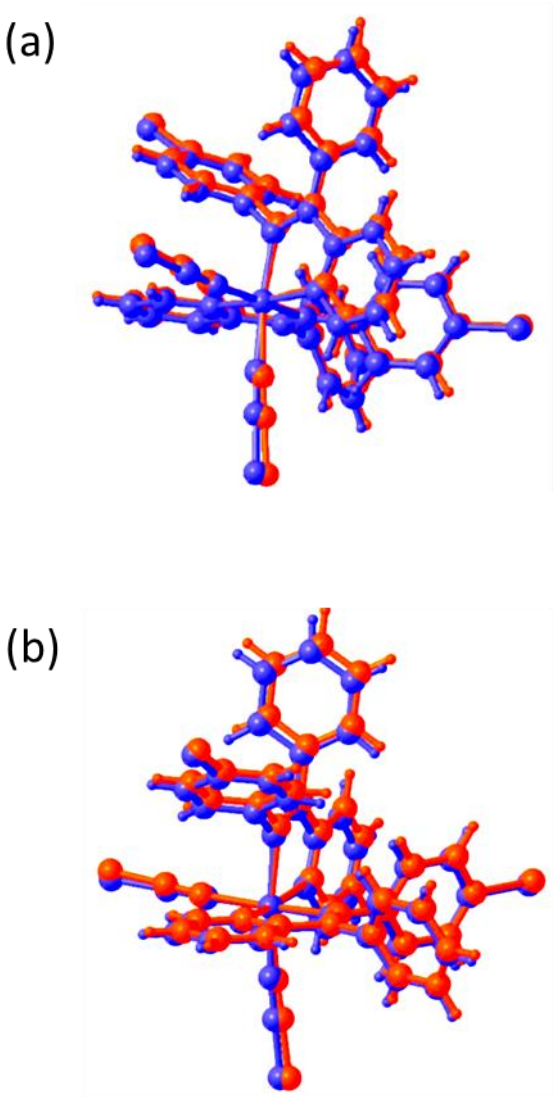

The crystal structures of **3** were also determined at 150 K (**3**^{150K}), 250 K (**3**^{250K}), 400 K (**3**^{400K}), 420 K (**3**^{420K}) in warming mode and again at 250 K (**3**^{250Kcooling}), 90 K (**3**^{90Kcooling}) in cooling mode after heating the crystal at 420 K. In all cases, the complex crystallises in tetragonal system with a chiral space group $P4_12_12$ (**Table S8**). At 150 K and 250 K, the observed coordination sphere parameters (Fe-N bond, ζ, Σ, Θ) are in line with the LS state (**Table 2**). The coordination environment around iron(II) gradually changes from LS to HS (**Table 2**) state with increase in temperature from 250 K to 420 K. At 400 K and 420 K, the HS conversion is 72% and 81%, respectively for iron(II). This is in good agreement with the observed magnetic data (2.1 $cm^3.K.mol^{-1}$ at 400 K: 70% HS and 2.45 $cm^3.K.mol^{-1}$ at 420 K: 81% HS). When the crystal is cooled down to 90 K (**3**^{90Kcooling}) after heating at 420 K, the LS state of iron(II) is recovered (**Table 2**). The crystal deteriorated rapidly above 420 K; it is not possible to follow the structural evolution in the temperature range 420-475 K

compared to magnetic measurements. However, according to thermogravimetric analyses the water molecule is released in two steps between (i) 345-450K and (ii) 450-475K that probably causing the deviation in spin crossover behaviour in **3** at 450K and 475K.

Table 2 Evolution of the relevant coordination sphere parameters for **3**

	$\mathbf{3}^{150K}$	$\mathbf{3}^{250K}$	$\mathbf{3}^{400K}$	$\mathbf{3}^{420K}$	$\mathbf{3}^{250Kcooling}$	$\mathbf{3}^{90Kcooling}$
Fe-N (Å)	1.9595(15)	1.958(3)	2.104(3)	2.116(4)	1.958(3)	1.956(3)
	1.9487(15) 1.9488(15)	1.948(3)	2.146(3)	2.177(4)	1.956(3)	1.949(3)
	1.9553(17) 1.9552(17)	1.958(3)	2.047(5)	2.058(6)	1.956(3)	1.947(3)
<Fe-N> (Å)	1.954(2)	1.955(3)	2.099(4)	2.117(5)	1.957(3)	1.951(3)
ζ (Å)	0.028	0.032	0.210	0.238	0.007	0.020
Σ (°)	39.1	39.9	65.9	68.8	40.4	39.0
Θ (°)	132	132	190	198	136	132
V(FeN_6) Å^3	9.868	9.892	12.034	12.332	9.889	9.802
Spin state	LS	LS	HS (72%)	HS (81%)	LS	LS

Crystal packing in 1-3

In the crystalline state of **1-3**, individual molecules are connected to each other through weak (pyridine)C-H···C(NCS) contacts involving two NCS moieties and two pyridine rings of two neighbouring molecules (**Tables 3-5**) along crystallographic *c*-axis forming an 1D-helical chain (**Figure 8**). Further, these 1D-helical chains are linked through weak (NCS)S···H-C(aniline) and weak intermolecular (aniline)C···H-C(phenyl) interactions along *ab*-plane leading to a 3D-network structure (**Figure 8**). It is found that iron(II) centres are in relatively close proximity along *c*-axis (intra-chain Fe-Fe distances) but in *ab*-plane iron(II) centres (inter-chain Fe-Fe distances) are widely separated. Moreover, the inclusion of large phenyl group in PPMA ligands leading the complexes to crystallise in tetragonal system with chiral space group either $P4_32_12$ (for **1**) or $P4_12_12$ (for **2** and **3**) in contrast to the complexes with PM-L ligands. Also, the supramolecular arrangement of 1D-helical chains diminishes the possibilities of π-π stacking as well as weakens major intermolecular contacts (NCS)S···C(phenyl groups-Schiff base) as compared to the reported complexes of PM-L ligands. This crystal packing is primarily responsible for non-cooperative gradual spin crossover in complexes **1-3**.

Figure 8 A view of Left: 1D-helical chain formed through (pyridine)C-H···C(NCS) and Right: Crystal packing where adjacent 1D-helical chains are connected through primarily (NCS)S···H-C(phenyl/aniline) and C-H···C(aniline/phenyl) interactions in **1**

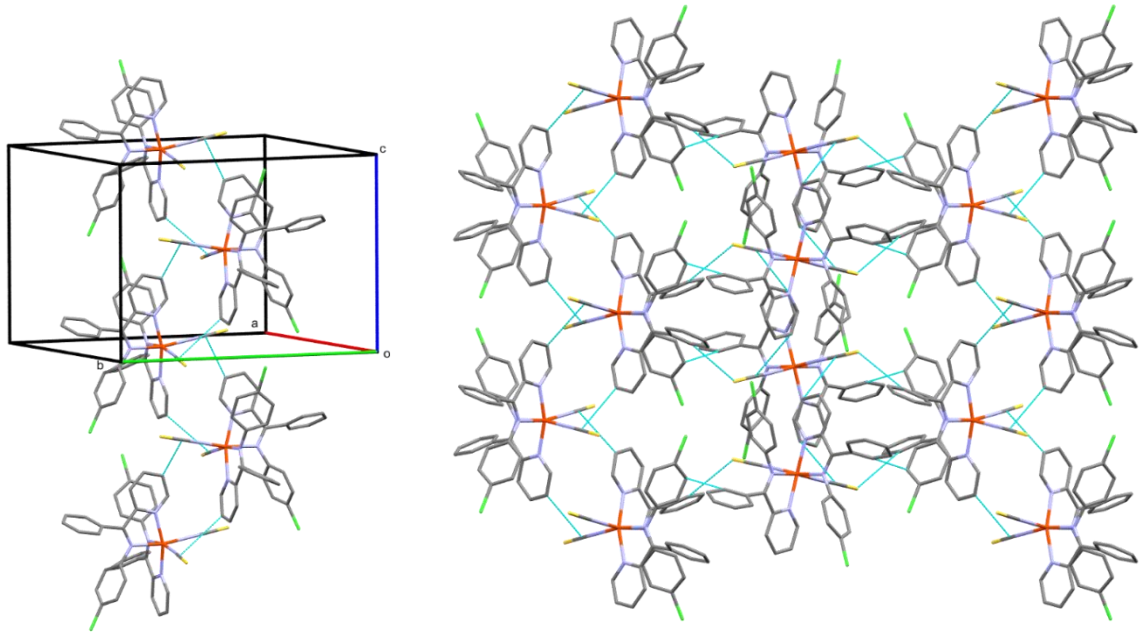

Table 3 Reorganisation of inter-molecular contacts in **1**

Contact	**1**^{150K}	**1**^{250K}	**1**^{300K}	**1**^{350K}	**1**^{400K}	**1**^{450K}
(pyridine)C-H···C(NCS)	2.785	2.774	2.790	2.786	2.797	2.796
Fe···Fe(Intra-chain)	7.641	7.681	7.685	7.655	7.608	7.590
(NCS)S···H-C(aniline)	3.012	2.990	3.029	3.022	2.996	3.011
C-H···C(aniline/phenyl)	2.960	3.016	3.017	3.024	3.011	3.021
Fe···Fe(Inter-chain)	10.749	10.805	10.833	10.927	11.016	11.097

Table 4 Reorganisation of inter-molecular contacts in **2**

Contact	**2**^{150K}	**2**^{250K}	**2**^{300K}	**2**^{350K}	**2**^{400K}	**2**^{450K}
(pyridine)C-H···C(NCS)	2.784	2.795	2.803	2.792	2.940	2.990
Fe···Fe(Intra-chain)	7.639	7.658	7.669	7.634	7.600	7.603
(NCS)S···H-C(aniline)	3.026	3.024	3.026	3.000	3.034	3.081
C-H···C(aniline/phenyl)	3.048	3.091	3.117	3.086	3.127	3.119
Fe···Fe(Inter-chain)	10.823	10.867	10.910	10.954	11.067	11.140

Table 5 Reorganisation of inter-molecular contacts in **3**

Contact	**3**^{150K}	**3**^{250K}	**3**^{400K}	**3**^{420K}	**3**^{250Kcooling}	**3**^{90Kcooling}

(pyridine)C-H···C(NCS)	2.730	2.758	2.917	2.935	2.789	2.723
Fe···Fe(Intra-chain)	7.658	7.670	7.686	7.682	7.700	7.658
(NCS)S···H-C(aniline)	2.999	3.042	3.137	3.156	2.996	2.966
C-H···C(aniline/phenyl)	2.977	3.020	3.061	3.066	3.031	2.986
Fe···Fe(Inter-chain)	10.768	10.820	10.985	11.019	10.760	10.660

Conclusions

Here, we have synthesised three new molecular *bis*-(thiocyanato)iron(II) complexes with judiciously designed bidentate N-donor Schiff bases of 2-Benzoylpyridine and 4-chloroaniline/4-bromoaniline/4-methylaniline. A relatively strong ligand field of the Schiff bases stabilises the LS state of iron(II) up to 300 K. Complexes **1** and **2** exhibit complete but gradual spin crossover behaviour ($T_{1/2} \approx 375$ K and 380 K) between 300 K and 500 K. On the contrary, complex **3** shows complete and non-cooperative spin crossover behaviour with some unusual irreversible features between 300 K and 475 K. For **3**, the spin crossover is reversible and gradual in nature between 90 K (LS) and 400 K (72% HS) as is evident of crystallographic parameters. First deviation occurs at 450 K upon cooling. Upon further warming at 475 K the complex exhibits a HS state of iron(II) that is stable down to 300 K upon further cooling. Below this temperature, it converts gradually to LS state on cooling. The equilibrium temperatures for first warming ($T_{1/2}\uparrow$) and second cooling ($T_{1/2}\downarrow$) are 375 K and 200 K, respectively. The structural modification and reorganisation of intermolecular contacts as well as loss of water molecule in complexes **1-3** were monitored through variable-temperature crystallographic evidences between 150-450 K (**1** and **2**) and 90-420 K (**3**) and thermogravimetric analyses. It is worth mentioning that de-hydration at higher temperature in complexes **1** and **2** creates some minor irreversible ligand motion which may be responsible for slight deviation in spin crossover. On the other hand, the de-hydration at high temperature in complex **3** causes strong irreversibility in spin crossover behaviour.

Experimental

Materials and methods

2-Benzoylpyridine (Sigma-Aldrich), 4-chloroaniline (Spectrochem, India), 4-bromoaniline (Spectrochem, India), 4-methylaniline (Spectrochem, India),

$Fe(ClO_4)_2 \cdot 6H_2O$ (Alfa-Aesar), KSCN (Spectrochem) and ascorbic acid (Spectrochem, India), were purchased from respective concerns and used as received. All the solvents used in the reactions were distilled and dried following common procedures. All the reactions were carried out under nitrogen atmosphere. Elemental analyses were carried out using Thermo-Scientific Flash 2000 CHNS/O Elemental Analyzer. Infrared spectra were recorded at room temperature using Thermo Nicolet, Avatar 370 FTIR spectrometer in 4000-400 cm^{-1} range (STIC, Cochin, India). UV-Vis spectra were recorded at room temperature on Agilent Technologies Cary 100 UV-Vis spectrophotometer equipped with multiple cell-holders. The ^{1}H-NMR spectra were recorded in $CDCl_3$ solvent on Bruker-500 MHz spectrometer. Mass spectra were recorded using XEVO G2-S-QTof waters corporation, USA, mass spectrometer (MNIT, Jaipur, India). Powder-XRD data of complexes **1-3** were collected by PANalytical, Empyrean Neatherlands set up using CuK_α radiation (λ = 1.54 Å). TGA data were recorded between 30-800 °C on TGA-DTA Perkin Elmer STA6000, Perkin Elmer Diamond instrument (CASE, IIT Jodhpur, India).

Synthesis of Schiff bases

The Schiff bases were synthesized using the following procedure. To the dry methanol solution (25 mL) of 2-benzoylpyridine (0.366 g, 2 mmol), a stoichiometric amount of aniline derivatives [4-chloroaniline (0.254 g, 2 mmol) for **Cl-PPMA**, 4-bromoaniline (0.344 g, 2 mmol) for **Br-PPMA** and 4-methylaniline (0.214 g, 2 mmol) for **CH_3-PPMA**] were added and refluxed for 24 h under nitrogen atmosphere. The yellowish brown solution was concentrated on a steam bath and dried in *vacuo* over $CaCl_2$ to get brown oil-like compound for subsequent use. However, all ligands were used for the preparation of iron(II) compound without further purification.

4-Chloro-N-(phenyl(pyridin-2-yl)methylene)aniline (Cl-PPMA)

Molecular formula $C_{18}H_{13}ClN_2$ (292.0767). Yield: 505 mg (86.35%); ESI-MS (in CH_3OH): m/z = 293.0847 [Calcd. 293.0840 for $(Cl\text{-}PPMA + H)^+$]. ^{1}H-NMR (δ/ppm, $CDCl_3$): 6.60 (2H), 7.10 (2H), 7.50 (3H), 7.60 (1H), 7.92 (1H), 8.06 (3H), 8.74 (1H). UV-Vis (λ_{max}/nm in CH_3OH; $\varepsilon/M^{-1}cm^{-1}$): 248 ($1.21 \times 10^4$), 347 ($1.75 \times 10^2$).

4-Bromo-N-(phenyl(pyridin-2-yl)methylene)aniline (Br-PPMA)

Molecular formula $C_{18}H_{13}BrN_2$ (336.0262). Yield: 598 mg (88.77%); ESI-MS (in CH_3OH): *m/z* = 337.0334 [Calcd. 337.0335 for (Br-PPMA+H)$^+$]. ^{1}H-NMR (δ/ppm, $CDCl_3$): 6.57 (2H), 7.23 (2H), 7.49 (3H), 7.60 (1H), 7.91 (1H), 8.06 (3H), 8.73 (1H). UV-Vis (λ_{max}/nm in CH_3OH; ε/$M^{-1}cm^{-1}$): 247 (1.54×10^4), 346 (4.49×10^2).

4-Methyl-N-(phenyl(pyridin-2-yl)methylene)aniline (CH_3-PPMA)

Molecular formula $C_{19}H_{16}N_2$ (272.1313). Yield: 491 mg (90.24%); ESI-MS (in CH_3OH): *m/z* = 273.1389 [Calcd. 273.1386 for (CH_3-PPMA+H)$^+$]. ^{1}H-NMR (δ/ppm, $CDCl_3$): 2.24 (3H), 6.61 (1H), 6.96 (1H), 7.49 (4H), 7.60 (1H), 7.91 (1H), 8.06 (4H), 8.73 (1H). UV-Vis (λ_{max}/nm in CH_3OH; ε/$M^{-1}cm^{-1}$): 261 (1.05×10^4), 346 (5.6×10^2).

Synthesis of complexes 1-3

Complexes **1-3** were prepared following a reported method[21, 22] with little modification. Under nitrogen atmosphere, iron(II) perchlorate hexahydrate, $Fe(ClO_4)_2 \cdot 6H_2O$ (0.254 g, 1 mmol) and potassium thiocyanate, KSCN, (0.194 g, 2 mmol) were dissolved in 15 mL freshly distilled methanol in presence of ascorbic acid to prevent the oxidation of iron(II). The colourless solution of $Fe(NCS)_2$ was separated from the white precipitate of potassium perchlorate by filtration, and added drop wise to a stoichiometric amount of Schiff base [Cl-PPMA (0.584 g, 2 mmol) for **1**, Br-PPMA (0.674 g, 2 mmol) for **2** and CH_3-PPMA (0.544 g, 2 mmol) for **3**] taken in 10 mL distilled methanol. The resulting intense blue solution was filtered and kept for slow evaporation in inert atmosphere. After 3-4 days needle (for **1-3**) shaped dark blue crystals were obtained. The crystalline compounds were collected by filtration and washed with cold methanol and dried under vacuum.

$[Fe(Cl\text{-}PPMA)_2(NCS)_2].H_2O$ (1)

Yield: 500 mg (64.47%); $C_{38}H_{28}N_6OS_2Cl_2Fe$ (775.54): calcd. C: 58.85, H: 3.64, N: 10.84, S: 8.27; found: 58.50, H: 3.45, N: 10.76, S: 8.72%. FTIR (KBr disc, cm^{-1}): 3440, 3050, 2890, 2814, 2100, 2060, 1590, 1480, 1445, 1398, 1336, 1256, 1161, 1085, 1011, 841, 800, 739, 694, 640, 597, 519, 432, 403. UV-Vis (λ_{max}/nm in CH_3OH; ε/$M^{-1}cm^{-1}$): **Cl-PPMA** based π→π* transitions: 258 (2.01×10^4), 340 (4.13×10^3); MLCT transitions: 530 (7.26×10^2) (shoulder) and 585 (1.05×10^3) (broad peak).

[Fe(Br-PPMA)$_2$(NCS)$_2$].H$_2$O (2)

Yield: 480 mg (55.52%); $C_{38}H_{28}N_6OS_2Br_2Fe$ (864.45): calcd. C: 52.80, H: 3.26, N: 9.72, S: 7.42; found: C: 52.74, H: 3.25, N: 9.71, S: 7.78%. FTIR (KBr disc, cm^{-1}): 3453, 3059, 2878, 2096, 2057, 1625, 1475, 1443, 1389, 1337, 1257, 1160, 1065, 996, 838, 800, 7.43, 695, 594, 513, 405. UV-Vis (λ_{max}/nm in CH_3OH; $\varepsilon/M^{-1}cm^{-1}$): **Br-PPMA** based $\pi\rightarrow\pi^*$ transitions = 258 (2.32×10^4), 340 (5.03×10^3); MLCT transitions = 530 (7.85×10^2) (shoulder) and 585 (1.42×10^3) (broad peak).

[Fe(CH$_3$-PPMA)$_2$(NCS)$_2$].H$_2$O (3)

Yield: 300 mg (41.08%); $C_{40}H_{34}N_6OS_2Fe$ (730.21): calcd. C: 65.39, H: 4.66, N: 11.44, S: 8.73; found: C: 65.41, H: 4.54, N: 11.51, S: 9.05%. FTIR (KBr disc, cm^{-1}): 3459, 3025, 2899, 2818, 2097, 2057, 1583, 1498, 1446, 1336, 1255, 1162, 1107, 1068, 1017, 983, 834, 797, 740, 692, 600, 537, 403. UV-Vis (λ_{max}/nm in CH_3OH; $\varepsilon/M^{-1}cm^{-1}$): **CH$_3$-PPMA** based $\pi\rightarrow\pi^*$/$n\rightarrow\pi^*$ transitions = 272 (8.17×10^3), 340 (2.52×10^3); MLCT transitions = 530 (1.36×10^3) (shoulder) and 585 (2.24×10^3) (broad peak).

Single crystal X-ray data collection and refinements

Structure determination at room temperature

Single-crystal X-ray data for **1-3** were collected at 293(2) K using an Agilent Technologies SuperNova Dual diffractometer equipped with an Atlas detector using $Mo_{K\alpha}$ radiation (λ = 0.71073 Å). The data were processed using *CrysAlisPro*.[35] The structures were solved by direct methods implemented in *SHELXT*[36] and refined by a full-matrix least-squares procedure based on F^2 with *SHELXL2017*.[37] All the non-hydrogen atoms were refined anisotropically. Hydrogen atoms were readily located in difference Fourier maps and were subsequently treated as riding atoms in geometrically idealized positions with U_{iso}(H) = kU_{eq}(C), where k = 1.5 for methyl groups, which were permitted to rotate but not to tilt, and 1.2 for all other H atoms unless otherwise noted. The room temperature structures are denoted as **1^{RT}, 2^{RT}** and **3^{RT}**.

Structure determination at variable temperatures

For variable temperature structural studies, suitable single crystals for **1-3** were selected from magnetic samples. The X-ray diffraction data were collected on Bruker

APEX-II with graphite monochromated $Mo_{K\alpha}$ radiation (λ = 0.7017 Å), equipped with CCD detectors and an Oxford instruments nitrogen cryo-stream. Structures were solved using a direct methods with *Olex2*.[38] Space group was checked by *Platon* software.[39] For **1** and **2**, data were collected on the full sphere at 150 K ($\mathbf{1}^{\mathbf{150K}}$ and $\mathbf{2}^{\mathbf{150K}}$) then at 250 K ($\mathbf{1}^{\mathbf{250K}}$ and $\mathbf{2}^{\mathbf{250K}}$), 300 K ($\mathbf{1}^{\mathbf{300K}}$ and $\mathbf{2}^{\mathbf{300K}}$), 350 K ($\mathbf{1}^{\mathbf{350K}}$ and $\mathbf{2}^{\mathbf{350K}}$), 400 K ($\mathbf{1}^{\mathbf{400K}}$ and $\mathbf{2}^{\mathbf{400K}}$) and 450 K ($\mathbf{1}^{\mathbf{450K}}$ and $\mathbf{2}^{\mathbf{450K}}$) on a single crystal. Above 450 K the stability of crystal was lost. In $\mathbf{1}^{\mathbf{450K}}$, there are some 'B level' errors, including large U(iso) of H (H2, H3, H4, H9), large flack X, low bond precision, small distance of C7--C12. For **3**, data were first collected on full sphere at 150 K ($\mathbf{3}^{\mathbf{150K}}$) then at 250 K ($\mathbf{3}^{\mathbf{250K}}$), 400 K ($\mathbf{3}^{\mathbf{400K}}$) and 420 K ($\mathbf{3}^{\mathbf{420K}}$) on a single crystal. This crystal was then save apart. Another crystal was used to find out the stability. Above 420 K, the stability of the crystal was lost. So, after warming at 420 K, crystal structures were recorded at 250 K ($\mathbf{3}^{\mathbf{250Kcooling}}$) and 90 K ($\mathbf{3}^{\mathbf{90Kcooling}}$) using the first crystal. Electron density associated with disordered solvent molecules was removed by solvent mask. Therefore, the chemical formula and crystal data given in Tables S5 and S8 do not take into account these solvent molecules.

Caution! A particular caution had to be taken for these X-ray diffraction data collections. All the compounds crystallize in a chiral space group and since both chiral forms of the crystals cannot be distinguished by a sole unit-cell check, a full data collection and structural determination is always needed to know the space group. Consequently, all the temperature dependence should be made on the same crystal. After checking the stability of the crystal for each compound a suitable single crystal was selected for X-ray diffraction to run the whole set of data collection. It also means that if one single-crystal breaks during a measurement the full process of the variable temperature study must be re-done on a new crystal. This time-consuming experimental protocol is the guarantee for reliable structural data.

Magnetic measurements

Magnetic measurements were performed using a MPMS 7XL SQUID Magnetometer from Quantum design, operating at 20 kOe of applied magnetic field, on 12.40 mg (for **1**), 10.83 mg (for **2**) and 11.24 mg (for **3**) of samples prepared in a polypropylene bag. The temperature was scanned from 10 K to 400 K at a sweeping rate of 3 K/min (for

1), in a settle mode (for **2**) and 4 K/min (for **3**). The photoswithcing was recorded directly into the SQUID magnetometer through an optical fibre placed close to the sample (6 cm). Irradiation is applied on a thin layer of compound and the relaxation temperature T(LIESST) is recorded according to the already reported protocol.[33, 34, 40] Further, the magnetic data up to 500 K (for **1-3**) were recorded using Microsense EZ7 Vibrating Sample Magnetometer with the 150-1000 K EV1-LNA temperature control option. Samples were weighed in aluminium capsules that were wrapped closed, and glued to a 3 mm ∅ quartz rod with double-face scotch tape. The measurements were performed under 15 kOe magnetic field at a temperature sweeping rate of 5 K/min. Nitrogen gas flow was used for temperature control. The diamagnetic corrections were made using Pascal's constants.[41] Let us note that compound **3** was recorded in the SQUID as a fresh sample and after 1h at 450 K in an oven.

Conflicts of interest

There are no conflicts to declare.

Acknowledgements

AKS acknowledges CSIR project grant (ref.: 01(3084)/21/EMR-II), SERB project grant (EMR/2016/001452) and DST-INSPIRE research grant (IFA-13, CH-97). KB is grateful to DST-SERB for NPDF research grant (PDF/2017/000929). VNR acknowledges Central University of Rajasthan, India for fellowship. FP is grateful for financial support from the Slovenian Research Agency (ARRS) through project P1-0175. We thank the EN-FIST Centre of Excellence, Ljubljana, Slovenia, for using SuperNova diffractometer for the data collections. Authors acknowledge the instrumental facilities through DST-FIST Grant (grant ref.: SR/FST/CSI-257/2014(c)) at Department of Chemistry, Central University of Rajasthan, India. The instrumental facilities at MNIT, Jaipur, India and STIC, Cochin, India are also gratefully acknowledged. The CNRS, University of Bordeaux and X-Ray facility service of the ICMCB are kindly acknowledged. The CNRS, the University of Bordeaux and the Région Aquitaine are also acknowledged as well the CSC and IDEX Bordeaux program for funding. Authors also thank Dr. V. Raghavendra Reddy, UGC-DAE Consortium for Scientific Research, Indore, India, for room temperature Mössbauer studies of complexes (**1-3**). The Central Instrumental Facilities (CIF) at Central

University of Rajasthan for powder-XRD studies is gratefully acknowledged. Authors also acknowledge the valuable contribution of Late Dr. Sunil G. Naik to this work.

Notes and references

‡The supporting information contains Mössbauer spectral data, room temperature powder-XRD, room and variable temperature X-ray crystallographic data, thermogravimetric analyses for **1-3**.

§CCDC No: 1978235-1978237 for $\mathbf{1}^{RT}$-$\mathbf{3}^{RT}$, 1979597, 1979599-1979600, 1979602, 1979604 and 2009216 for **1**, 1979605, 1979607-1979609, 1979611, 2009217 for **2** and 1979617-1979618 and 1979620-1979623 for **3** contain the supplementary crystallographic data. These data can be obtained free of charge from The Cambridge Crystallographic Data Centre via www.ccdc.cam.ac.uk/data_request/cif or by contacting The Cambridge Crystallographic Data Centre, 12 Union Road, Cambridge CB2 1EZ, UK; fax: +44 1223 336033.

1. O. Kahn and C. J. Martinez, Spin-transition polymers: from molecular materials toward memory devices, *Science*, 1998, **279**, 44-48.
2. P. Gütlich and H. A. Goodwin, in *Spin Crossover in Transition Metal Compounds I*, Springer, 2004, pp. 1-47.
3. A. Bousseksou, G. Molnár and G. Matouzenko, Switching of molecular spin states in inorganic complexes by temperature, pressure, magnetic field and light: towards molecular devices, *European Journal of Inorganic Chemistry*, 2004, **2004**, 4353-4369.
4. P. Gamez, J. S. Costa, M. Quesada and G. Aromí, Iron Spin-Crossover compounds: from fundamental studies to practical applications, *Dalton Transactions*, 2009, 7845-7853.
5. C. Lefter, V. Davesne, L. Salmon, G. Molnár, P. Demont, A. Rotaru and A. Bousseksou, Charge transport and electrical properties of spin crossover materials: towards nanoelectronic and spintronic devices, *Magnetochemistry*, 2016, **2**, 18.
6. K. S. Kumar and M. Ruben, Sublimable Spin- Crossover Complexes: From Spin- State Switching to Molecular Devices, *Angewandte Chemie International Edition*, 2021, **60**, 7502-7521.
7. K. Ridier, A.-C. Bas, Y. Zhang, L. Routaboul, L. Salmon, G. Molnár, C. Bergaud and A. Bousseksou, Unprecedented switching endurance affords for high-resolution surface temperature mapping using a spin-crossover film, *Nature communications*, 2020, **11**, 1-9.
8. J. F. Dayen, N. Konstantinov, M. Palluel, N. Daro, M. Soliman, G. Chastanet, B. Doudin and B. Kundys, Room temperature optoelectronic device operating with spin crossover nanoparticles, *Materials Horizons*, 2021.
9. S. Zheng, N. R. Reintjens, M. A. Siegler, O. Roubeau, E. Bouwman, A. Rudavskyi, R. Havenith and S. Bonnet, Stabilization of the low-spin state in a mononuclear iron

(II) complex and high-temperature cooperative spin crossover mediated by hydrogen bonding, *Chemistry-A European Journal*, 2016, **22**, 331-339.
10. K. S. Kumar, Y. Bayeh, T. Gebretsadik, F. Elemo, M. Gebrezgiabher, M. Thomas and M. Ruben, Spin-crossover in iron (II)-Schiff base complexes, *Dalton Transactions*, 2019, **48**, 15321-15337.
11. W. Nicolazzi and A. Bousseksou, Thermodynamical aspects of the spin crossover phenomenon, *Comptes Rendus Chimie*, 2018, **21**, 1060-1074.
12. M. G. Reeves, E. Tailleur, P. A. Wood, M. Marchivie, G. Chastanet, P. Guionneau and S. Parsons, Mapping the cooperativity pathways in spin crossover complexes, *Chemical Science*, 2021, **12**, 1007-1015.
13. H. Spiering, Elastic interaction in spin-crossover compounds, *Spin Crossover in Transition Metal Compounds III*, 2004, 171-195.
14. C. Enachescu and W. Nicolazzi, Elastic models, lattice dynamics and finite size effects in molecular spin crossover systems, *Comptes Rendus Chimie*, 2018, **21**, 1179-1195.
15. P. Guionneau, M. Marchivie and G. Chastanet, Multiscale Approach of Spin Crossover Materials: A Concept Mixing Russian Dolls and Domino Effects, *Chemistry–A European Journal*, 2021, **27**, 1483-1486.
16. P. Guionneau, Crystallography and spin-crossover. A view of breathing materials, *Dalton Transactions*, 2014, **43**, 382-393.
17. P. Guionneau, M. Marchivie, G. Bravic, J.-F. Létard and D. Chasseau, in *Spin Crossover in Transition Metal Compounds II*, Springer, 2004, pp. 97-128.
18. E. Tailleur, M. Marchivie, N. Daro, G. Chastanet and P. Guionneau, Thermal spin-crossover with a large hysteresis spanning room temperature in a mononuclear complex, *Chemical Communications*, 2017, **53**, 4763-4766.
19. E. Tailleur, M. Marchivie, P. Negrier, D. Denux, S. Massip, D. Mondieig, G. Chastanet and P. Guionneau, Using polymorphism to master the spin crossover mechanism in [Fe (PM-PeA) 2 (NCSe) 2], *CrystEngComm*, 2019, **21**, 6246-6251.
20. W. Guo, N. Daro, S. b. Pillet, M. Marchivie, E. E. Bendeif, E. Tailleur, K. Chainok, D. Denux, G. Chastanet and P. Guionneau, Unprecedented reverse volume expansion in spin- transition crystals, *Chemistry–A European Journal*, 2020, **26**, 12927-12930.
21. J.-F. Létard, P. Guionneau, E. Codjovi, O. Lavastre, G. Bravic, D. Chasseau and O. Kahn, Wide Thermal Hysteresis for the Mononuclear Spin-Crossover Compound cis-Bis (thiocyanato) bis [N-(2 '-pyridylmethylene)-4-(phenylethynyl) anilino] iron (II), *Journal of the American Chemical Society*, 1997, **119**, 10861-10862.
22. J.-F. Létard, P. Guionneau, L. Rabardel, J. A. Howard, A. E. Goeta, D. Chasseau and O. Kahn, Structural, magnetic, and photomagnetic studies of a mononuclear iron (II) derivative exhibiting an exceptionally abrupt spin transition. Light-induced thermal hysteresis phenomenon, *Inorganic chemistry*, 1998, **37**, 4432-4441.
23. P. Guionneau, J.-F. Létard, D. S. Yufit, D. Chasseau, G. Bravic, A. E. Goeta, J. A. Howard and O. Kahn, Structural approach of the features of the spin crossover transition in iron (II) compounds, *Journal of Materials Chemistry*, 1999, **9**, 985-994.
24. J.-F. Létard, M. Kollmansberger, C. Carbonera, M. Marchivie and P. Guionneau, Structural, magnetic and photomagnetic study of the [Fe (PM–NEA) 2 (NCS) 2] spin crossover complex, *Comptes Rendus Chimie*, 2008, **11**, 1155-1165.
25. J.-F. Létard, G. Chastanet, O. Nguyen, S. Marcén, M. Marchivie, P. Guionneau, D. Chasseau and P. Gütlich, Spin crossover properties of the [Fe (PM-BiA) 2 (NCS) 2] complex–Phases I and II, *Monatshefte für Chemie/Chemical Monthly*, 2003, **134**, 165-182.

26. C.-F. Wang, Z.-S. Yao, G.-Y. Yang and J. Tao, Ligand Substituent Effects on the Spin-Crossover Behaviors of Dinuclear Iron (II) Compounds, *Inorganic chemistry*, 2019, **58**, 1309-1316.
27. P. Gütlich, Y. Garcia and H. A. Goodwin, Spin crossover phenomena in Fe (ii) complexesDedicated to Professor FA Cotton on occasion of his 70th birthday, *Chemical Society Reviews*, 2000, **29**, 419-427.
28. N. Suryadevara, A. Pausch, E. Moreno- Pineda, A. Mizuno, J. Bürck, A. Baksi, T. Hochdörffer, I. Šalitroš, A. S. Ulrich and M. M. Kappes, Chiral Resolution of Spin- Crossover Active Iron (II)[2x2] Grid Complexes, *Chemistry–A European Journal*, 2021, **27**, 15172-15180.
29. C. Bartual-Murgui, L. Pineiro-Lopez, F. J. Valverde-Muñoz, M. C. Muñoz, M. Seredyuk and J. A. Real, Chiral and racemic spin crossover polymorphs in a family of mononuclear Iron (II) compounds, *Inorganic chemistry*, 2017, **56**, 13535-13546.
30. T.-T. Ma, X.-P. Sun, Z.-S. Yao and J. Tao, Homochiral versus racemic polymorphs of spin-crossover iron (ii) complexes with reversible LIESST effect, *Inorganic Chemistry Frontiers*, 2020, **7**, 1196-1204.
31. R. Ketkaew, Y. Tantirungrotechai, P. Harding, G. Chastanet, P. Guionneau, M. Marchivie and D. J. Harding, OctaDist: a tool for calculating distortion parameters in spin crossover and coordination complexes, *Dalton Transactions*, 2021, **50**, 1086-1096.
32. S. Decurtins, P. Gütlich, C. P. Köhler, H. Spiering and A. Hauser, Light-induced excited spin state trapping in a transition-metal complex: The hexa-1-propyltetrazole-iron (II) tetrafluoroborate spin-crossover system, *Chemical physics letters*, 1984, **105**, 1-4.
33. G. Chastanet, C. Desplanches, C. Baldé, P. Rosa, M. Marchivie and P. Guionneau, A critical review of the T (LIESST) temperature in spin crossover materials− What it is and what it is not, *Chemistry Squared-Chem2*, 2018, **2**, 2.
34. J.-F. Létard, L. Capes, G. Chastanet, N. Moliner, S. Létard, J.-A. Real and O. Kahn, Critical temperature of the LIESST effect in iron (II) spin crossover compounds, *Chemical physics letters*, 1999, **313**, 115-120.
35. , Rigaku Oxford Diffraction, C. P., Rigaku Corporation, Tokyo, Japan, 2015.
36. G. M. Sheldrick, SHELXT–Integrated space-group and crystal-structure determination, *Acta Crystallographica Section A: Foundations and Advances*, 2015, **71**, 3-8.
37. G. M. Sheldrick, Crystal structure refinement with SHELXL, *Acta Crystallographica Section C: Structural Chemistry*, 2015, **71**, 3-8.
38. O. V. Dolomanov, L. J. Bourhis, R. J. Gildea, J. A. Howard and H. Puschmann, OLEX2: a complete structure solution, refinement and analysis program, *Journal of applied crystallography*, 2009, **42**, 339-341.
39. A. Spek, Single-crystal structure validation with the program PLATON, *Journal of Applied Crystallography*, 2003, **36**, 7-13.
40. G. Chastanet, C. Desplanches, M. Gonidec, P. Guionneau, M. Marchivie, C. Mathonière and P. Rosa, Light-induced excited spin-state trapping: a methodological approach.*Journal*, 2019.
41. G. A. Bain and J. F. Berry, Diamagnetic corrections and Pascal's constants, *Journal of Chemical Education*, 2008, **85**, 532.